

Double-White-Dwarf Merger Products among High-Mass White Dwarfs

Sihao Cheng (程思浩),¹ Jeffrey D. Cummings,¹ Brice Ménard,^{1,2} and Silvia Toonen³

¹*Department of Physics and Astronomy, The Johns Hopkins University, 3400 N Charles Street, Baltimore, MD 21218, USA*

²*Kavli Institute for the Physics and Mathematics of the Universe, University of Tokyo, Kashiwa 277-8583, Japan*

³*Institute for Gravitational Wave Astronomy, School of Physics and Astronomy, West office 237, Birmingham B15 2TT, Edgbaston, UK*

Abstract

Double-white-dwarf (double-WD) binaries may merge within a Hubble time and produce high-mass WDs. Compared to other high-mass WDs, the double-WD merger products have higher velocity dispersion because they are older. With the power of *Gaia* data, we show strong evidence for double-WD merger products among high-mass WDs by analyzing the transverse-velocity distribution of more than a thousand high-mass WDs ($0.8 - 1.3 M_{\odot}$). We estimate that the fraction of double-WD merger products in our sample is about 20%. We also calculate the double-WD merger rate and its mass dependence. Our results agree with binary population synthesis results and support the idea that double-WD mergers can contribute to a large fraction of type-Ia supernovae.

Keywords: White dwarf stars, Stellar kinematics, Stellar ages, Type Ia supernovae, Bayesian statistics

1. Introduction

During the last decades, there has been increasing evidence showing that a large number of double-white-dwarf (double-WD) systems should merge within a Hubble time (e.g., [Badenes & Maoz 2012](#); [Brown et al. 2016](#); [Maoz et al. 2018](#)). Many double-WD mergers are believed to produce new white dwarfs with higher masses (e.g., [Lorén-Aguilar et al. 2009](#)). So, a fraction of high-mass white dwarfs in the solar neighbourhood are expected to be double-WD merger products (e.g., [Toonen et al. 2017](#); [Timmink et al. 2019](#)). To verify the existence of these merger products, some investigators have looked for an excess of high-mass white dwarfs ([Giammichele et al. 2012](#); [Rebassa-Mansergas et al. 2015](#); [Tremblay et al. 2016](#)), and others have searched for kinematic signatures of these merger products ([Wegg & Phinney 2012](#); [Dunlap & Clemens 2015](#)). The kinematic method makes use of the following facts: high-mass double-WD merger products are in general older than singly-evolved white dwarfs because of their binary evolution, and according to the age–velocity–dispersion relation (AVR) of the milky-way disc (e.g., [Nordström et al. 2004](#)), these older double-WD merger products have higher velocity dispersion. The former method, based on number counts, is influenced by large systematic errors from the adopted initial–final-mass relation of white dwarfs and the sample completeness. In

contrast, the kinematic method is less influenced by systematic errors, but it was limited by the sample size of white dwarfs with kinematic measurements.

Thanks to the European Space Agency *Gaia* mission ([Gaia Collaboration et al. 2016](#)), the number of stars with precise kinematic measurements has been enlarged drastically. [Cheng et al. \(2019\)](#) selected a deep, homogeneous sample of white dwarfs in a narrow mass range ($1.08 - 1.23 M_{\odot}$) from *Gaia* Data Release 2 (DR2, [Gaia Collaboration et al. 2018a](#)) to investigate the ‘Q branch’, an over-density of white dwarfs on the Hertzsprung–Russell (H–R) diagram, which is caused by a cooling anomaly. As a byproduct of their kinematic analysis, the fraction of double-WD merger products among white dwarfs in their mass range were inferred to be about 22%, and they reserve the task of conducting an analysis optimized for detecting double-WD merger products and discussions on this topic to this paper.

In this paper, we extend the kinematic analysis of high-mass white dwarfs to a wider mass range and adopt a more realistic delay-time distribution for binary evolution. We estimate the fractions of double-WD merger products as a function of mass and calculate the corresponding merger rates. We then compare our results to predictions from binary population synthesis. We also discuss the implication of our results for the progenitor problem of type-Ia supernovae (SNIa), as the double-WD merger is a promising scenario of type-Ia supernova explosion (e.g., [Webbink 1984](#); [Iben & Tutukov 1984](#)).

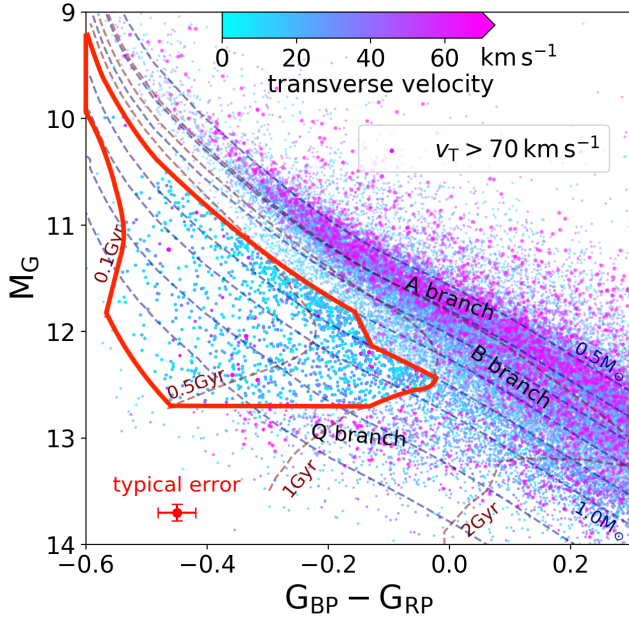


Figure 1. The H–R diagram of WDs in *Gaia* DR2. We show a 250 pc sample of WDs with high quality measurements and a grid of WD masses m_{WD} and photometric ages τ_{phot} derived from the combined O/Ne-core and C/O-core WD cooling model. WDs evolve along their cooling tracks, i.e., the constant-mass curves. The red region includes 1380 nearby, high-mass, hot WDs selected in Section 2 for our kinematic analysis.

2. Data

Gaia DR2 provides accurate astrometric (Lindgren et al. 2018) and photometric (Riello et al. 2018; Evans et al. 2018) measurements for more than one billion of stars. To search for the kinematic signature of double-WD merger products efficiently, we select nearby, high-mass, hot white dwarfs with precise astrometric and photometric measurements from the *Gaia* DR2 white dwarf catalog compiled by Gentile Fusillo et al. (2019). Below, we introduce in detail our sample selection and the derivation of white dwarf parameters.

We first impose the same quality cuts as equations (1)–(5) in Cheng et al. (2019) and a distance cut:

$$1000 / \text{parallax} < 250 \quad (1)$$

to select white dwarfs with high-precision astrometric and photometric measurements. These cuts do *not* introduce any *explicit* kinematic biases to our white dwarf sample.

Then, as the kinematic signature of double-WD merger products most outstanding among high-mass, hot (young-photometric-age) white dwarfs, we carry out selections on the photometric mass (m_{WD}) and age (τ_{phot}) of white dwarfs. These cuts, equivalent to cuts on the H–R diagram, are designed to both maximize the sample size and minimize contamination from the standard-mass helium-atmosphere white dwarfs (the ‘B branch’, Gaia Collaboration et al.

2018b):

$$\begin{aligned} &0.8 M_{\odot} < m_{\text{WD}} < 0.9 M_{\odot}, \\ &0.1 \text{ Gyr} < \tau_{\text{phot}} < 0.7 \text{ Gyr}; \\ &\text{or} \\ &0.9 M_{\odot} < m_{\text{WD}} < 1.28 M_{\odot}, \\ &0.1 \text{ Gyr} < \tau_{\text{phot}} < 1.0 \text{ Gyr}. \end{aligned} \quad (2)$$

The white dwarf parameters m_{WD} and τ_{phot} are derived in the following way. First, we define the absolute magnitude M_G as $M_G = G + 5 \log(\varpi / \text{mas}^{-1}) - 10$, where G and ϖ are the G band magnitude and parallax. Then, we convert the H–R diagram coordinate into m_{WD} and cooling time t_{cool} by interpolating a grid of cooling tracks for C/O-core DA white dwarfs (Fontaine et al. 2001) and synthetic colors (Holberg & Bergeron 2006; Kowalski & Saumon 2006; Tremblay et al. 2011)¹². For white dwarfs heavier than $1.07 M_{\odot}$ we use cooling tracks of O/Ne white dwarfs (Camisassa et al. 2019). Finally, the photometric age τ_{phot} is obtained by adding the cooling time t_{cool} to the main-sequence age, which we calculate based on an initial–final mass relation (Cummings et al. 2018) and the relation between pre-cooling time and main-sequence mass from Choi et al. (2016) for non-rotating, solar-metallicity stars.

As shown by Cheng et al. (2019), the ‘Q branch’ on the H–R diagram is produced by an anomalous cooling behavior: some white dwarfs stop cooling and stay on the branch for 8 Gyr, which creates both an over-density and a high velocity excess. To avoid modelling the influence of this cooling delay on the velocity distribution and only focus on the binary-evolution delay for double-WD mergers, we exclude the ‘Q branch’ region on the H–R diagram with the following cut:

$$M_G < 12.7. \quad (3)$$

The selection region on the H–R diagram and the 1380 selected objects of white dwarfs are shown in Figure 1.

Given the distance and luminosity cut, our sample is nearly volume limited, because $M_G < 12.7$ corresponds to an apparent magnitude $G < 19.7$ at 250 pc, which is brighter than where the completeness of *Gaia* DR2 drops (Arenou et al. 2018). In addition, we find that our quality cuts only exclude less than 5% of the objects, given the distance and H–R diagram cuts in Equations 1–3.

We divide our selected sample into 5 mass bins, based on the aforementioned photometric mass (assuming C/O core below $1.07 M_{\odot}$ and O/Ne core above it). The edges of

¹ <http://www.astro.umontreal.ca/~bergeron/CoolingModels/>.

² We make a python 3 module for this kind of transformations publicly available on https://github.com/SihaoCheng/WD_models.

bins are 0.8, 0.9, 1.0, 1.1, 1.2, 1.28 M_{\odot} . If instead one believes some white dwarfs heavier than 1.07 M_{\odot} still have C/O cores, then these mass bins correspond to 0.8, 0.9, 1.0, 1.14, 1.24, 1.24, 1.32 M_{\odot} . The sample sizes in these mass bins are 408, 431, 322, 169, and 50, respectively. Because of the absolute-magnitude cut and pre-WD evolution times, the photometric-age ranges for the five samples are different. We estimate them to be 0.42, 0.82, 0.86, 0.66, 0.42 Gyr, respectively.

Finally, we derive the kinematics of white dwarfs, which are related to the true ages of white dwarfs through the age-velocity-dispersion relation. Since *Gaia* does not provide radial velocity information for white dwarfs due to the narrow wavelength coverage of its spectrometer (Gaia Collaboration et al. 2016), we focus on the two components of transverse velocity $\mathbf{v}_T = (v_L, v_B)$:

$$v_L = \frac{\mu_L - (A \cos 2l + B) \cos b}{\varpi}, \quad (4)$$

$$v_B = \frac{\mu_B + A \sin 2l \sin b \cos b}{\varpi}, \quad (5)$$

where μ_L and μ_B are the proper motion in the Galactic longitude and latitude directions, and A and B are the Oort constants taken from Bovy (2017).

3. Model

Our goal is to measure the amount of double-WD merger products among high-mass white dwarfs using the kinematic information. According to the age-velocity-dispersion relation, a group of stars with older true stellar age (τ) has higher velocity dispersion. On the other hand, one can derive the photometric isochrone age (τ_{phot}) of white dwarfs from the H-R diagram. If a white dwarf evolves in isolation, τ_{phot} should be equal to τ , whereas if it originates from a double-WD merger event, then an age discrepancy

$$\Delta t \equiv \tau - \tau_{\text{phot}} > 0 \quad (6)$$

will be created from binary evolution. In general, a white dwarf produced from binary evolution may have positive or negative Δt , but for double-WD mergers with high total mass, the discrepancy is almost always positive (Timmink et al. 2019). So, for a given τ_{phot} , double-WD merger products are older and have higher velocity dispersion.

Following Wegg & Phinney (2012) and Cheng et al. (2019), we assume that the double-WD merger ‘resets’ the white dwarf back to a sufficiently high temperature, so that the real cooling time is equal to the photometric cooling time. Then, Δt can also be expressed as the difference of pre-cooling times between the two evolutionary scenarios, $\Delta t = (\tau - t_{\text{cool}}) - (\tau_{\text{phot}} - t_{\text{cool}})$, where t_{cool} is the cooling time, and the first item $\tau - t_{\text{cool}}$ is sometimes called the ‘delay time’ of double-WD merger. It has been widely used that the

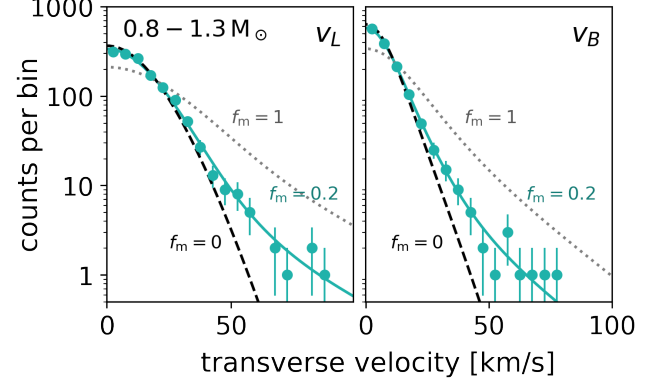


Figure 2. The velocity distribution of our white dwarf sample. We show the sample of white dwarfs from all five mass bins (0.8 – 1.3 M_{\odot}) as an example. v_L and v_B in the left and right panel of the figure means the Galactic longitude and latitude components of the transverse velocity. We present the observed histograms of the absolute values of v_L and v_B in 20 bins between 0 and 100 km s^{-1} and Poisson errors. We also show the theoretical velocity distributions for $f_m = 0, 1$, and the average of best-fitting values weighted by the sample size in each mass bin, which is about 0.2. Note that the y-axes are on logarithmic scale.

distribution of the age discrepancy, $p(\Delta t)$, for double-WD mergers with high total masses is approximately a power law, i.e., $p(\Delta t) \approx \Delta t^{-1}$ (Maoz et al. 2010), because the binary delay time $\tau - t_{\text{cool}}$ is dominated by the double-WD phase when the orbit shrinks due to gravitational-wave emission, and the single-star pre-cooling time $\tau_{\text{phot}} - t_{\text{cool}}$ is negligible. However, in our mass ranges, none of the two statements are valid. So, we use more realistic distributions for Δt , with the binary delay-time distribution, $p(\tau - t_{\text{cool}})$, obtained from binary population synthesis (see Appendix A for details) and the values of $\tau_{\text{phot}} - t_{\text{cool}}$ from Section 2.

We consider our white dwarf sample as a mixture of two populations: singly-evolved white dwarfs and double-WD merger products³, with fractions $1 - f_m$ and f_m , respectively. If f_m is higher, the tail of the velocity distribution will also be higher, because the double-WD merger products are on average older. For the velocity distribution, we assume that stars with the same true age τ have a Gaussian velocity distribution $\mathbf{v} \sim \mathcal{N}(\mathbf{v}_0(\tau), \Sigma(\tau))$ relative to the Sun (e.g., Binney & Tremaine 2008). The size of this Gaussian distribution is determined by τ through the age-velocity-dispersion relation, and the center of this Gaussian distribution is determined by the solar motion and the age-dependent asymmetric drift ($\sigma_U(\tau)^2/80 \text{ km s}^{-1}$).

³ The high-mass white dwarfs originating from other types of mergers such as main-sequence and giant star mergers have much shorter age discrepancy Δt than that of double-WD mergers. So, in terms of kinematics, we treat the merger products of other types the same as singly-evolved white dwarfs.

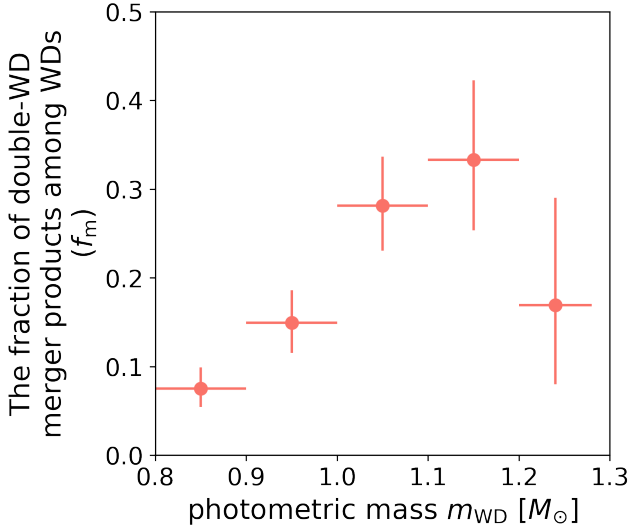


Figure 3. Our estimates for the fraction of double-WD merger products among high-mass white dwarfs, in five bins of white dwarf photometric mass. The sample sizes in these mass bins, from lower to higher masses, are 408, 431, 322, 169, and 50, respectively.

We use the same Bayesian framework as constructed by Cheng et al. (2019) to infer the fraction f_m from the photometric age τ_{phot} and transverse velocity v_T of each white dwarf. This model uses the conditional probability of v_T given τ_{phot} and other observables as the likelihood function, and thus it eliminates spatial selection biases. In the model, we set f_m and the solar motion as free parameters and adopt the best-fitting age–velocity–dispersion relation in Cheng et al. (2019), a flat star formation history in our sample volume, and the delay-time distribution of double-WD mergers shown in Appendix A. We do not need to model the ‘extra cooling delay’ included in Cheng et al. (2019) because this delay has no effect in our selected region. We do not include white dwarf kick effects in our model, because for single-evolved white dwarfs, the kick velocity during the white dwarf formation is less than 1 km s^{-1} (El-Badry & Rix 2018), and for double-WD mergers, the kick velocity during merger is a few km s^{-1} Dan et al. (e.g., 2014), which have only tiny contribution to the increase of velocity dispersion compared to the contribution from the binary-evolution delay.

4. Results and Discussions

4.1. Constraints on the fraction of merger products

With a thirty-time larger sample of high-mass white dwarfs selected from *Gaia* DR2, we are allowed to go beyond Wegg & Phinney (2012) and set strong constraints on f_m . Figure 2 illustrates the transverse-velocity distribution of white dwarfs in our sample. The clear velocity excess is strong evidence for the existence of double-WD merger products. For clarity we only show the distribution of the whole sample, i.e., the

combination of all five mass bins, but similar results can be found in each single mass bin, too. In Figure 3, we show our estimate of f_m in each mass bin. We find that the fraction of double-WD mergers in our mass range of $0.8 - 1.3 M_{\odot}$ varies from 10% to 35%, with an average of about 20%. This fraction is roughly constant as a function of mass, though declines at the two end are suggested.

To test the robustness of our results, we check for the influence of sample selection, the adopted star formation history, and the adopted age–velocity–dispersion relation in our model. We found that a different distance cut such as 200 pc or 300 pc cuts and a linearly decreasing star formation history with 5 times higher rate at 11 Gyrs ago have less than 20% fractional influence on the estimate of f_m . For the influence of the age–velocity–dispersion relation, our results are mostly influenced by the 0–4 Gyr part, where the delay-time distribution is peaked. Adopting the high velocity dispersion from Just & Jahreiß (2010) as used by Wegg & Phinney (2012) will reduce f_m by a factor of 2, but given the observational constraints from both main-sequence stars (e.g., Nordström et al. 2004) and white dwarfs (Cheng et al. 2019), such high values of velocity dispersion are unlikely. The effect of adopted delay-time distribution can be seen from the comparison between our results in the mass range of $1.08 - 1.23 M_{\odot}$ and that of Cheng et al. (2019): adopting a power-law delay-time distribution, they obtain a result about 30% lower. So, we estimate the fractional systematic error of our results as 30% (a factor of 0.7–1.3). Our estimate of f_m is consistent with population synthesis results (Temink et al. 2019).

4.2. Double-white-dwarf merger rate

The fraction of double-WD merger products (f_m) obtained in Section 4.1 can be translated into double-WD merger rates. Since our sample is nearly volume limited, the merger rate in each mass bin is estimated by:

$$\text{merger rate} = \frac{f_m \cdot N}{m_{\star} \cdot \Delta\tau_{\text{phot}}}, \quad (7)$$

where N is the sample size of each mass bin (listed in the caption of Figure 3), m_{\star} the stellar mass of the milky way within 250 pc, and $\Delta\tau_{\text{phot}}$ the photometric-age range of each mass bin, as is estimated in Section 2. The stellar mass m_{\star} is estimated to be $4.1 \times 10^6 M_{\odot}$, using the local stellar mass density $\rho_{\star} = 0.083 M_{\odot} \text{ pc}^{-3}$ (McMillan 2011) and a scale-height 300 pc of the disc. We show our estimates of the current double-WD merger rate in Figure 4. The total merger rate in our mass range amounts to $0.7 \times 10^{-13} M_{\odot}^{-1} \text{ yr}^{-1}$.

We take the mass of merger products as the total mass of the original double-WD binary. This is true for CO-CO white dwarf mergers (e.g., Dan et al. 2014) but not for He-CO white dwarf mergers, which may lose significant amount of mass during the R Coronae Borealis phase and produce

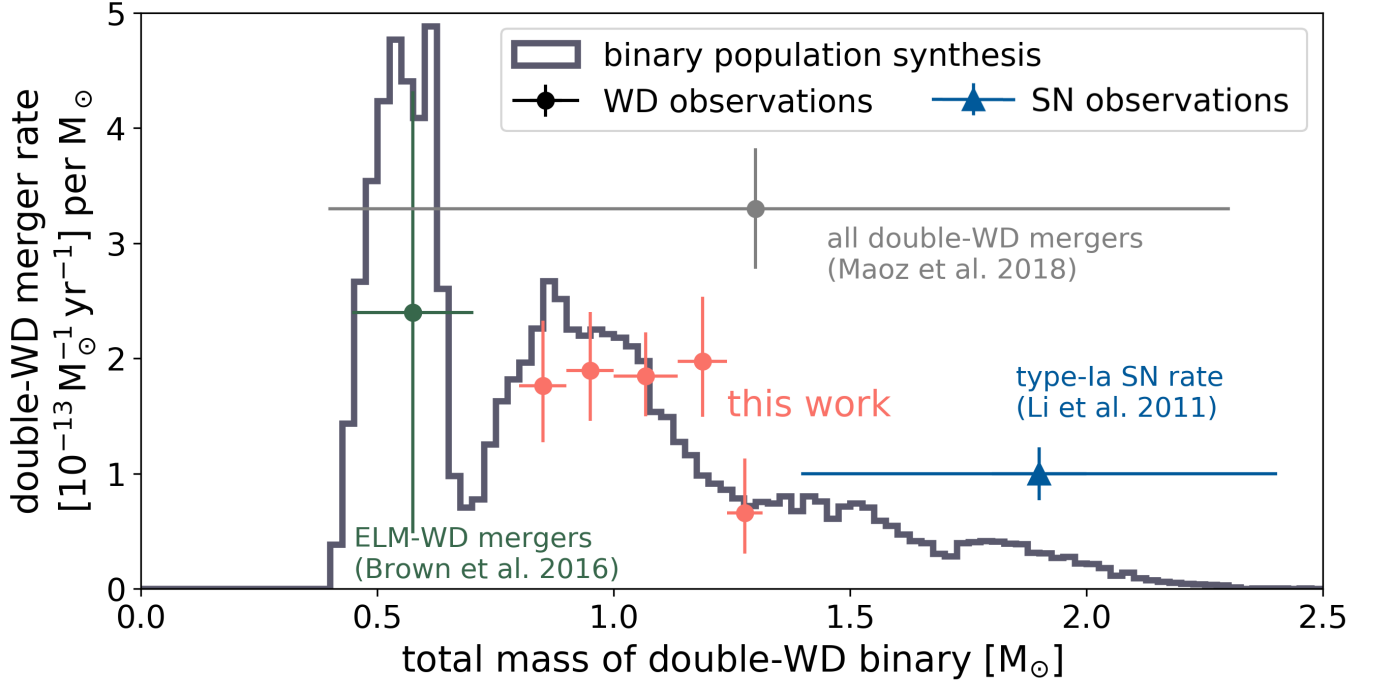


Figure 4. A comparison of the observed and simulated double-WD merger rate. The red data points with error bars are our observational estimates based on double-WD merger products. The histogram shows binary population synthesis results of current merger rate, given a flat star formation history. Other data points show estimates in the literature based on the orbital distribution of observed double-WD systems: the light-grey one is an estimate for all double-WD mergers (Maoz et al. 2018), and the green one is for systems with at least one extremely-low-mass (ELM, $< 0.3 M_{\odot}$) WD (Brown et al. 2016). In our population synthesis, almost all systems with the total mass lower than about $0.7 M_{\odot}$ have at least one ELM member. The blue data point shows the observed SNIa rate. Comparisons between a data point and the histogram should be made in terms of the area under the horizontal ‘error-bar’ of the data point and the area under the histogram in the same mass range.

white dwarfs with $0.6 - 0.7 M_{\odot}$ (Schwab 2019). So, we are likely to underestimate the merger rate of systems with original mass below $1.0 M_{\odot}$, where He-CO white dwarf mergers become important.

In Figure 4 we also show the merger rate from binary population synthesis, with a flat star-formation history assumed. If a decreasing star-formation rate was assumed, as the delay-time distribution is low for mergers with a long delay time, the synthesis would predict a lower current merger rate than plotted in Figure 4. Details of the population synthesis are shown in Appendix A. We find that the synthesized merger rates agree well with our observational estimates without any tuning of parameters. Note that in our analysis of *Gaia* white dwarfs, we only use the *distribution* of the delay time but never use the total merger rate information from the population synthesis. So, the match between the observed and synthesized merger rate is not a circular argument but rather a validation of our understanding of binary evolution.

For comparison, we also plot in Figure 4 other estimates of the double-WD merger rate in the literature. While we count the products of mergers, other estimates are obtained from observing pre-merger systems and predicting the merger rate. Maoz et al. (2012); Badenes & Maoz (2012); Maoz & Hallakoun (2017); Maoz et al. (2018) extrapolates the or-

bitual distribution of double-WD binaries to estimate the total double-WD merger rate, with an up-to-date estimate being $(6.3 \pm 1.0) \times 10^{-13} M_{\odot}^{-1} \text{yr}^{-1}$. Brown et al. (2016) estimate the merger rate of double-WD binaries with at least one extremely-low-mass (ELM) white dwarf to be $3 \times 10^{-3} \text{yr}^{-1}$ in the milky way, corresponding to $0.5 \times 10^{-13} M_{\odot}^{-1} \text{yr}^{-1}$, with an 80% to 110% uncertainty. As these numbers address the merger rates of systems in different mass ranges, one cannot compare them directly. But, if we are allowed to use the mass distribution from binary population synthesis to scale these estimates, we will find that the merger rate obtained by Maoz et al. (2018) is about 3 times of our estimates, and the estimate from Brown et al. (2016) is consistent with our results within uncertainty, as illustrated in Figure 4. As discussed in Maoz et al. (2018), if the merger rates are so high as their estimate, almost all high-mass white dwarfs will need to be double-WD merger products, which is hard to believe given the velocity distribution we observe. Nevertheless, it is worth noting that the observational constraints of the double-WD merger rate have converged to within a factor of a few.

In summary, our estimates of the double-WD merger rate provide a validation for current binary population synthesis. These estimates add significant precision and mass resolution to our knowledge of the double-WD merger rate.

4.3. Implication for type-Ia supernovae

Type-Ia supernovae are important distance indicators, element factories, interstellar medium heaters, and cosmic-ray accelerators, but their progenitors remain unclear (e.g., Maoz et al. 2014). The double-WD merger is a promising scenario of type-Ia supernova (e.g., Webbink 1984; Iben & Tutukov 1984; Tutukov et al. 1992; Maoz et al. 2010; Menekens et al. 2010; Sato et al. 2015; Liu et al. 2017; Shen et al. 2018a,b; Perets et al. 2019). The comparison between double-WD merger rate and the type-Ia supernova rate is a critical test from this scenario. When a flat star formation history is assumed, our population synthesis (Appendix A) provides a merger rate of about $0.3 \times 10^{-13} \text{ M}_{\odot}^{-1} \text{ yr}^{-1}$ for super-Chandrasekhar double-WD systems, which is about 1/7 of the total synthesized double-WD merger rate and consistent with previous studies (e.g., Ruiter et al. 2009; Yungelson & Kuranov 2017). For the D^6 (dynamically-driven double-degenerate double-detonation) scenario (e.g., Shen et al. 2018a), a lower rate is obtained, because it requires in general higher total mass of the system (see figure 2 of Shen et al. 2017).

On the other hand, the observed type-Ia supernova rate for a Milky-Way-like galaxy (Sb-Sbc type) is $(1.0 \pm 0.3) \times 10^{-13} \text{ M}_{\odot}^{-1} \text{ yr}^{-1}$ (Li et al. 2011), or $1.3 \times 10^{-3} \text{ M}_{\odot}^{-1}$ in terms of a time-integrated rate (Maoz & Graur 2017). This is close to, though 2-3 times higher than, the synthesized rate for the super-Chandra and D^6 double-WD merger scenario. As discussed in Section 4.2, our estimates of the double-WD merger rate within $0.8 - 1.3 \text{ M}_{\odot}$ are in agreement with population synthesis results. So, if we are allowed to extrapolate according to the mass distribution of mergers from simulations, then

- our measurements support the idea that double-WD mergers contribute a large fraction to type-Ia supernovae;
- if all type-Ia supernovae come from double-WD mergers, it seems that there exist other explosion mechanisms whose requirement on the total mass of the binary is lower than the Chandrasekhar- and D^6 explosion models.

5. Conclusion

The merger of two white dwarfs in a close binary system may result in a new white dwarf with higher mass. Therefore, among the high-mass white dwarfs observed today, a fraction should come from double-WD mergers. Experiencing binary evolution, these merger products have older true ages than their photometric isochrone ages. According to the age-velocity-dispersion relation in the milky-way disc, older stars have higher velocity dispersion. So, the fraction

of double-WD merger products (f_m) can be estimated from the velocity distribution of high-mass white dwarfs.

We select a homogeneous sample of high-mass white dwarfs ($0.8 - 1.3 \text{ M}_{\odot}$, $d < 250 \text{ pc}$) from *Gaia* DR2, which includes 1380 objects. Our sample is about thirty times larger than that of a previous study with a similar idea (Wegg & Phinney 2012). We infer f_m in five mass bins using a Bayesian model of white dwarf transverse velocities. We find

- about 20% of white dwarfs in our mass range come from double-WD mergers;
- the corresponding double-WD merger rates in our mass range add up to $0.7 \times 10^{-13} \text{ M}_{\odot}^{-1} \text{ yr}^{-1}$.

We show f_m and the merger rate as a function of mass in Figures 3 and 4, respectively. We estimate our systematic error to be within 30% (a factor of 0.7-1.3). Our results are in good agreement with the predictions from binary population synthesis (see Appendix A).

Our estimates add significant precision and mass resolution to our knowledge of the double-WD merger rate. If it is allowed to extrapolate the estimates to a higher mass range, our results suggest that double-WD mergers can contribute to a large fraction of type-Ia supernovae.

In a few years, the increasing astrometric and photometric precision provided by future *Gaia* data releases and the radial velocity measurements of white dwarfs by future surveys such as SDSS-V (e.g., Kollmeier et al. 2017) will enlarge the available sample size of high-mass white dwarfs and allow for even tighter constraints. We are starting to be able to reliably and precisely compare the observed double-WD merger rates with binary population synthesis, which will shed light upon the progenitor problem of type-Ia supernovae.

Acknowledgments

SC thanks Siyu Yao for her constant encouragement and inspiration. JC would like to acknowledge his support from the National Science Foundation (NSF) through grant AST-1614933. BM thanks the David and Lucile Packard Foundation. ST acknowledges support from the Netherlands Research Council NWO (grant VENI [nr. 639.041.645]).

This work has made use of data from the European Space Agency (ESA) mission *Gaia* (<https://www.cosmos.esa.int/gaia>), processed by the *Gaia* Data Processing and Analysis Consortium (DPAC, <https://www.cosmos.esa.int/web/gaia/dpac/consortium>). Funding for the DPAC has been provided by national institutions, in particular the institutions participating in the *Gaia* Multilateral Agreement.

Software: astropy package (Astropy Collaboration et al. 2013, 2018), emcee (Foreman-Mackey et al. 2013), numpy

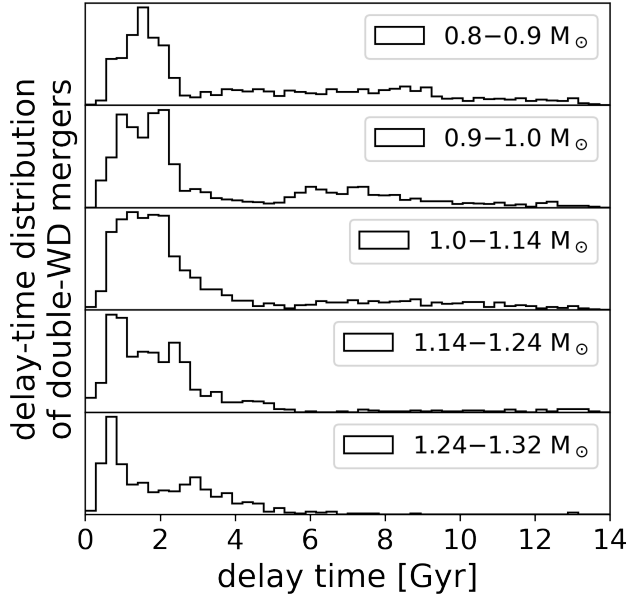


Figure A1. The delay-time distributions of double-WD mergers used in our model. These distributions are generated from binary population synthesis. The x-axis is the delay time of binary evolution, i.e., $\tau - t_{\text{cool}}$ for the resulting white dwarf. The y-axis is in linear scale and normalized to their maximum values. We input to our model the shapes of these five distributions as probability distribution and do not use the information from their normalization.

(Oliphant 2006), matplotlib (Hunter 2007), SciPy (Jones et al. 2001–)

Appendix A The binary population synthesis

Here we describe the binary population synthesis that we use in this paper to derive the delay-time distribution. The

models are synthesized using the binary population synthesis code *SeBa* (Portegies Zwart & Verbunt 1996; Toonen et al. 2012). The models are identical to the default models used in Toonen et al. (2017). We have adopted a Kroupa IMF (Kroupa et al. 1993) and a uniform mass ratio distribution between 0 and 1 (Raghavan et al. 2010; Duchêne & Kraus 2013). Furthermore, we assume a uniform distribution in the logarithmic semi-major axis up to $10^6 R_{\odot}$ (Abt 1983), and a thermal distribution of eccentricities between 0 and 1 (Heggie 1975).

One of the main sources of uncertainty in the synthetic populations (Toonen et al. 2014) is a phase of unstable mass transfer, i.e., the common-envelope (CE) phase (for a review Ivanova et al. 2013). Similar to Toonen et al. (2017), we apply the ‘ $\gamma\alpha$ ’ model. This model reproduces the mass ratio distribution (Toonen et al. 2012) and number density Toonen et al. (2017) of double-WD systems best. In the ‘ $\gamma\alpha$ ’ model, we apply the classical (α -)CE that is based on energy conservation (Webbink 1984), and the (γ -)modelling that is based on a balance of angular momentum (Nelemans et al. 2000). Regarding the former the parameters $\alpha\lambda = 2$ describe how efficient orbital energy can be used to unbind the envelope and how strong the envelope is bound to the donor star, and regarding the latter the parameter $\gamma = 1.75$ describes the efficiency of angular momentum usage. The γ -modelling is applied unless the binary contains a compact object or the CE is triggered by a tidal instability. We note that for our purpose to compare the merger rate, the delay-time distribution of the ‘ $\gamma\alpha$ ’ model does not significantly differ from that of the model that exclusively adopts the α -CE with $\alpha\lambda = 2$ (see Toonen et al. 2012).

Figure A1 shows the delay-time distributions in five mass bins, which are used in our kinematic analysis. For the synthesized merger rates shown in Figure 4, we in addition assume a 50% binary fraction of all stars (see also Duchêne & Kraus 2013; Moe & Di Stefano 2017).

References

- Abt, H. A. 1983, *ARA&A*, **21**, 343
Arenou, F., Luri, X., Babusiaux, C., et al. 2018, *A&A*, **616**, A17
Astropy Collaboration, Robitaille, T. P., Tollerud, E. J., et al. 2013, *A&A*, **558**, A33
Astropy Collaboration, Price-Whelan, A. M., Sipőcz, B. M., et al. 2018, *AJ*, **156**, 123
Badenes, C., & Maoz, D. 2012, *ApJL*, **749**, L11
Binney, J., & Tremaine, S. 2008, *Galactic Dynamics: Second Edition* (Princeton University Press)
Bovy, J. 2017, *MNRAS*, **468**, L63
Brown, W. R., Kilic, M., Kenyon, S. J., & Gianninas, A. 2016, *ApJ*, **824**, 46
Camisassa, M. E., Althaus, L. G., Córscico, A. H., et al. 2019, *A&A*, **625**, A87
Cheng, S., Cummings, J. D., & Ménard, B. 2019, arXiv e-prints, arXiv:1905.12710. <https://arxiv.org/abs/1905.12710>
Choi, J., Dotter, A., Conroy, C., et al. 2016, *ApJ*, **823**, 102
Cummings, J. D., Kalirai, J. S., Tremblay, P.-E., Ramirez-Ruiz, E., & Choi, J. 2018, *ApJ*, **866**, 21
Dan, M., Rosswog, S., Brüggen, M., & Podsiadlowski, P. 2014, *MNRAS*, **438**, 14
Duchêne, G., & Kraus, A. 2013, *ARA&A*, **51**, 269
Dunlap, B. H., & Clemens, J. C. 2015, in *Astronomical Society of the Pacific Conference Series*, Vol. **493**, 19th European Workshop on White Dwarfs, ed. P. Dufour, P. Bergeron, & G. Fontaine, 547
El-Badry, K., & Rix, H.-W. 2018, *MNRAS*, **480**, 4884

- Evans, D. W., Riello, M., De Angeli, F., et al. 2018, *A&A*, **616**, A4
- Fontaine, G., Brassard, P., & Bergeron, P. 2001, *PASP*, **113**, 409
- Foreman-Mackey, D., Hogg, D. W., Lang, D., & Goodman, J. 2013, *PASP*, **125**, 306
- Gaia Collaboration, Prusti, T., de Bruijne, J. H. J., et al. 2016, *A&A*, **595**, A1
- Gaia Collaboration, Babusiaux, C., van Leeuwen, F., et al. 2018a, *A&A*, **616**, A10
- Gaia Collaboration, Brown, A. G. A., Vallenari, A., et al. 2018b, *A&A*, **616**, A1
- Gentile Fusillo, N. P., Tremblay, P.-E., Gänsicke, B. T., et al. 2019, *MNRAS*, **482**, 4570
- Giammichele, N., Bergeron, P., & Dufour, P. 2012, *ApJS*, **199**, 29
- Heggie, D. C. 1975, *MNRAS*, **173**, 729
- Holberg, J. B., & Bergeron, P. 2006, *AJ*, **132**, 1221
- Hunter, J. D. 2007, *Computing in Science & Engineering*, **9**, 90
- Iben, Jr., I., & Tutukov, A. V. 1984, *ApJS*, **54**, 335
- Ivanova, N., Justham, S., Chen, X., et al. 2013, *A&A Rv*, **21**, 59
- Jones, E., Oliphant, T., Peterson, P., et al. 2001–, SciPy: Open source scientific tools for Python
- Just, A., & Jahreiß, H. 2010, *MNRAS*, **402**, 461
- Kollmeier, J. A., Zasowski, G., Rix, H.-W., et al. 2017, arXiv e-prints, arXiv:1711.03234. <https://arxiv.org/abs/1711.03234>
- Kowalski, P. M., & Saumon, D. 2006, *ApJL*, **651**, L137
- Kroupa, P., Tout, C. A., & Gilmore, G. 1993, *MNRAS*, **262**, 545
- Li, W., Chornock, R., Leaman, J., et al. 2011, *MNRAS*, **412**, 1473
- Lindgren, L., Hernández, J., Bombrun, A., et al. 2018, *A&A*, **616**, A2
- Liu, D., Wang, B., Wu, C., & Han, Z. 2017, *A&A*, **606**, A136
- Lorén-Aguilar, P., Isern, J., & García-Berro, E. 2009, *A&A*, **500**, 1193
- Maoz, D., Badenes, C., & Bickerton, S. J. 2012, *ApJ*, **751**, 143
- Maoz, D., & Graur, O. 2017, *ApJ*, **848**, 25
- Maoz, D., & Hallakoun, N. 2017, *MNRAS*, **467**, 1414
- Maoz, D., Hallakoun, N., & Badenes, C. 2018, *MNRAS*, **476**, 2584
- Maoz, D., Mannucci, F., & Nelemans, G. 2014, *ARA&A*, **52**, 107
- Maoz, D., Sharon, K., & Gal-Yam, A. 2010, *ApJ*, **722**, 1879
- McMillan, P. J. 2011, *MNRAS*, **414**, 2446
- Mennekens, N., Vanbeveren, D., De Greve, J. P., & De Donder, E. 2010, *A&A*, **515**, A89
- Moe, M., & Di Stefano, R. 2017, *ApJS*, **230**, 15
- Nelemans, G., Verbunt, F., Yungelson, L. R., & Portegies Zwart, S. F. 2000, *A&A*, **360**, 1011
- Nordström, B., Mayor, M., Andersen, J., et al. 2004, *A&A*, **418**, 989
- Oliphant, T. E. 2006, A guide to NumPy, Vol. 1 (Trelgol Publishing USA)
- Perets, H. B., Zenati, Y., Toonen, S., & Bobrick, A. 2019, arXiv e-prints, arXiv:1910.07532. <https://arxiv.org/abs/1910.07532>
- Portegies Zwart, S. F., & Verbunt, F. 1996, *A&A*, **309**, 179
- Raghavan, D., McAlister, H. A., Henry, T. J., et al. 2010, *ApJS*, **190**, 1
- Rebassa-Mansergas, A., Rybicka, M., Liu, X.-W., Han, Z., & García-Berro, E. 2015, *MNRAS*, **452**, 1637
- Riello, M., De Angeli, F., Evans, D. W., et al. 2018, *A&A*, **616**, A3
- Ruiter, A. J., Belczynski, K., & Fryer, C. 2009, *ApJ*, **699**, 2026
- Sato, Y., Nakasato, N., Tanikawa, A., et al. 2015, *ApJ*, **807**, 105
- Schwab, J. 2019, arXiv e-prints, arXiv:1909.02569. <https://arxiv.org/abs/1909.02569>
- Shen, K. J., Kasen, D., Miles, B. J., & Townsley, D. M. 2018a, *ApJ*, **854**, 52
- Shen, K. J., Toonen, S., & Graur, O. 2017, *ApJL*, **851**, L50
- Shen, K. J., Boubert, D., Gänsicke, B. T., et al. 2018b, *ApJ*, **865**, 15
- Temink, K. D., Toonen, S., Zapartas, E., Justham, S., & Gänsicke, B. T. 2019, arXiv e-prints, arXiv:1910.05335. <https://arxiv.org/abs/1910.05335>
- Toonen, S., Claeys, J. S. W., Mennekens, N., & Ruiter, A. J. 2014, *A&A*, **562**, A14
- Toonen, S., Hollands, M., Gänsicke, B. T., & Boekholt, T. 2017, *A&A*, **602**, A16
- Toonen, S., Nelemans, G., & Portegies Zwart, S. 2012, *A&A*, **546**, A70
- Tremblay, P.-E., Bergeron, P., & Gianninas, A. 2011, *ApJ*, **730**, 128
- Tremblay, P.-E., Cummings, J., Kalirai, J. S., et al. 2016, *MNRAS*, **461**, 2100
- Tutukov, A. V., Yungelson, L. R., & Iben, Jr., I. 1992, *ApJ*, **386**, 197
- Webbink, R. F. 1984, *ApJ*, **277**, 355
- Wegg, C., & Phinney, E. S. 2012, *MNRAS*, **426**, 427
- Yungelson, L. R., & Kuranov, A. G. 2017, *MNRAS*, **464**, 1607